

Peak structure in the interlayer conductance of Moiré superlattices

Yizhou Tao(陶懿洲), Chao Liu(刘超), Mingwen Xiao(肖明文), and Henan Fang(方贺男)

Citation: Chin. Phys. B, 2024, 33 (**10**): 107301. DOI: 10.1088/1674-1056/ad655b
Journal homepage: http://cpb.iphy.ac.cn; http://iopscience.iop.org/cpb

What follows is a list of articles you may be interested in

Gate-field control of valley polarization in valleytronics

Ting-Ting Zhang(张婷婷), Yilin Han(韩依琳), Run-Wu Zhang(张闰午), and Zhi-Ming Yu(余智明)
Chin. Phys. B, 2024, 33 (**6**): 067303. DOI: 10.1088/1674-1056/ad401a

Magnetic and magnetotransport properties of layered $TaCoTe_2$ single crystals

Ming Mei(梅明), Zheng Chen(陈正), Yong Nie(聂勇), Yuanyuan Wang(王园园), Xiangde Zhu(朱相德), Wei Ning(宁伟), and Mingliang Tian(田明亮)
Chin. Phys. B, 2023, 32 (**12**): 127303. DOI: 10.1088/1674-1056/acd10a

Effect of crystallographic orientations on transport properties of methylthiol-terminated permethyloligosilane molecular junction

Ming-Lang Wang(王明郎), Bo-Han Zhang(张博涵), Wen-Fei Zhang(张雯斐), Xin-Yue Tian(田馨月), Guang-Ping Zhang(张广平), and Chuan-Kui Wang(王传奎)
Chin. Phys. B, 2022, 31 (**7**): 077303. DOI: 10.1088/1674-1056/ac4cbf

Preparation of PSFO and LPSFO nanofibers by electrospinning and their electronic transport and magnetic properties

Ying Su(苏影), Dong-Yang Zhu(朱东阳), Ting-Ting Zhang(张亭亭), Yu-Rui Zhang(张玉瑞), Wen-Peng Han(韩文鹏), Jun Zhang(张俊), Seeram Ramakrishna, and Yun-Ze Long(龙云泽)
Chin. Phys. B, 2022, 31 (**5**): 057305. DOI: 10.1088/1674-1056/ac3baa

Research status and performance optimization of medium-temperature thermoelectric material SnTe

Pan-Pan Peng(彭盼盼), Chao Wang(王超), Lan-Wei Li(李岚伟), Shu-Yao Li(李淑瑶), and Yan-Qun Chen(陈艳群)
Chin. Phys. B, 2022, 31 (**4**): 047307. DOI: 10.1088/1674-1056/ac20c9

Peak structure in the interlayer conductance of Moiré superlattices

Yizhou Tao(陶懿洲)[1], Chao Liu(刘超)[1], Mingwen Xiao(肖明文)[2], and Henan Fang(方贺男)[1,†]

[1] *College of Electronic and Optical Engineering & College of Flexible Electronics (Future Technology), Nanjing University of Posts and Telecommunications, Nanjing* 210023, *China*
[2] *Department of Physics, Nanjing University, Nanjing* 210093, *China*

(Received 4 March 2024; revised manuscript received 7 July 2024; accepted manuscript online 19 July 2024)

We investigate the peak structure in the interlayer conductance of Moiré superlattices using a tunneling theory we developed previously. The theoretical results predict that, due to the resonance of two different partial waves, the double-peak structure can appear in the curve of the interlayer conductance versus twist angle. Furthermore, we study the influences of the model parameters, i.e., the chemical potential of electrodes, the thickness of Moiré superlattice, and the strength of interface potential, on the peak structure of the interlayer conductance. In particular, the parameter dependence of the peak structure is concluded via a phase diagram, and the physical meanings of the phase diagram is formulized. Finally, the potential applications of the present work is discussed.

Keywords: Moiré superlattice, interlayer conductance, electronic transport, twistronics

PACS: 73.43.Jn, 78.67.Pt, 72.80.Vp, 72.10.–d **DOI:** 10.1088/1674-1056/ad655b

1. Introduction

With the discovery of graphene,[1] two-dimensional (2D) materials have become a focal point in the fields of nanotechnology and condensed matter physics.[2–4] In particular, bilayer systems of 2D materials are widely studied. In bilayer systems, when the two layers are twisted at a specific angle, periodic Moiré patterns are formed, thus forming the so-called Moiré superlattices.[5–7] Compared to untwisted bilayer systems, the Moiré superlattices exhibit novel physical characteristics,[8,9] e.g., tunable Mott insulators,[10] unconventional superconductivity,[11] and atomic reconstruction.[12] The physical mechanisms underlying these characteristics are highly related to the interlayer coupling of two twisted layers.[13] As a characterization method commonly used, the measurement of interlayer conductance is a direct and reliable method to study the interlayer coupling of Moiré superlattices.

Experimentally, several research groups have investigated the relationship between the interlayer conductance and the twist angle in Moiré superlattices.[14–20] A common observational result across these studies is that the interlayer conductance decreases monotonically with the twist angle within the domain [0°, 30°]. In addition, in Refs. [16–18] researchers identified a sharp conductance peak around the twist angle of 21.8°. Overall, the interlayer conductance behaves like a continuously decreasing background plus one sharp peak within the domain [0°, 30°]. Nevertheless, for a long period of time, there has not yet been unified theoretical explanation to the background and the peak of interlayer conductance.

2. Method

Recently, we have developed a theory for Moiré superlattices based on the optical diffraction method.[21] Within the theoretical framework, the Moiré superlattice is regarded as a tunneling barrier, and the interlayer conductance is treated as tunneling conductance, due to the nearly insulation characteristics of 2D materials along the interlayer or longitudinal direction.[22] Correspondingly, the system to measure the interlayer conductance of the Moiré superlattice can be considered as a tunneling junction, which is schematically displayed in Fig. 1. Fortunately, this theory can provide a comprehensive interpretation for the interlayer conductance of the Moiré superlattices. It is found that the decreasing background of the interlayer conductance can be attributed to the increasing strength of the interface potential, and the peak originates from the resonance of scattering of tunneling electrons with the interface potential. Mathematically, the resonance occurs when the amplitude of transmitted wave function of the tunneling electron becomes divergent, and the amplitudes can be written as

$$A_1 = \frac{1}{2}\frac{\exp(\mathrm{i}k_{0z}^{+}\cdot d_1)}{1+\frac{\mathrm{i}m\gamma(\alpha)}{\hbar^2 k_{0z}^{+}}},\quad A_2 = \frac{1}{2}\frac{\exp(\mathrm{i}k_{hz}^{+}\cdot d_1)}{1+\frac{\mathrm{i}m\gamma(\alpha)}{\hbar^2 k_{hz}^{+}}}, \tag{1}$$

$$A_3 = \frac{1}{2}\frac{\exp(\mathrm{i}k_{0z}^{-}\cdot d_1)}{1+\frac{\mathrm{i}m\gamma(\alpha)}{\hbar^2 k_{0z}^{-}}},\quad A_4 = \frac{1}{2}\frac{\exp(\mathrm{i}k_{hz}^{-}\cdot d_1)}{1+\frac{\mathrm{i}m\gamma(\alpha)}{\hbar^2 k_{hz}^{-}}}, \tag{2}$$

where d_1 is the thickness of the upper layer of the Moiré superlattice, m is the mass of electron, α is the twist angle, and $\gamma(\alpha)$ represents the strength of the potential which approximately describes the effect from the interface. Thereinto, $\gamma(\alpha)=\gamma_0[1-\cos(6\alpha)]$, where γ_0 is a model parameter. In ad-

†Corresponding author. E-mail: fanghn@njupt.edu.cn

© 2024 Chinese Physical Society and IOP Publishing Ltd

dition, $k_{0z}^{\pm}$ and $k_{hz}^{\pm}$ are the z-components of wave vectors of the partial waves at the interface. Physically, the wave vectors of the partial waves at the interface can be divided into two types: (1) the wave vectors whose in-plane components are equal to that of the wave vector of the incident electron wave, i.e., $\boldsymbol{k}_0^{\pm}$. (2) the wave vectors whose in-plane components are equal to those of the wave vector of the incident electron wave plus a reciprocal lattice vector of the tunneling barrier, i.e., $\boldsymbol{k}_{\rm h}^{\pm}$. They can be expressed as

$$\boldsymbol{k}_0^{\pm} = \boldsymbol{k}_{\parallel} + \sqrt{\boldsymbol{k}^2 - \boldsymbol{k}_{\parallel}^2 - 2m\hbar^{-2}v(0) \pm 2m\hbar^{-2}v(\boldsymbol{K}_{\rm h})}\boldsymbol{e}_z, \tag{3}$$

$$\boldsymbol{k}_{\rm h}^{\pm} = \boldsymbol{k}_{\parallel} + \boldsymbol{K}_{\rm h} + \sqrt{\boldsymbol{k}^2 - (\boldsymbol{k}_{\parallel} + \boldsymbol{K}_{\rm h})^2 - 2m\hbar^{-2}v(0) \pm 2m\hbar^{-2}v(\boldsymbol{K}_{\rm h})}\boldsymbol{e}_z, \tag{4}$$

where $\boldsymbol{k}_{\parallel}$ denotes the normal projection of $\boldsymbol{k}$ in the lateral plane; $v(0)$ and $v(\boldsymbol{K}_{\rm h})$ correspond to the Fourier transform of the atomic potential of the barrier, with $\boldsymbol{K}_{\rm h}$ denoting the planar reciprocal lattice vector; $\boldsymbol{e}_z$ is the unit vector of z direction; $\boldsymbol{k}$ represents the incident wave vector, and the Fermi wave vector of the incident electrons is

$$k_{\rm F} = \sqrt{\frac{2me}{\hbar^2}\mu}, \tag{5}$$

where e represents the electron charge, and μ is the chemical potential of the electrodes. Due to the divergence of the amplitude of transmitted wave function, the conductance peak may bring abrupt change of the interlayer conductance with variation of the twist angle.

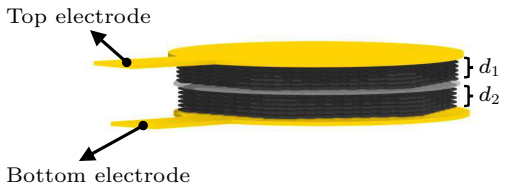


Fig. 1. Diagrammatic sketch of the studied system.

Under the parameters of our previous work, only A_3 is divergent, leading to a interlayer conductance curve with one single peak. In principle, A_2 and A_4 may also be divergent when the parameters vary. Accordingly, there will appear multiple peaks in the curve of interlayer conductance. The multiple-peak structure cannot only enrich the physical characteristics of Moiré superlattices, but also broaden the application of Moiré superlattices. Therefore, it is necessary to theoretically investigate the multiple-peak structure of the interlayer conductance of Moiré superlattices.

To this end, we shall, in the following, apply our theory to graphite/graphite Moiré superlattices, and investigate the multiple-peak structure of interlayer conductance. The details of the theory can be referred to the supplementary material. The model parameters of the graphite/graphite Moiré superlattices are the same as our previous work.[21]

3. Result and discussion

According to Eqs. (1)–(5), the chemical potential of the electrodes μ is the key parameter for the divergence of amplitudes of transmitted wave function. Therefore, we would like to first investigate the influences of μ on the peak structure of the interlayer conductance. The numerical results are displayed in Fig. 2(a), where $v(\boldsymbol{K}_{\rm h}) = 3.5$ eV, $v(0) = 3.12$ eV, $d_1 = d_2 = 30$ nm, and $\gamma_0 = 4 \times 10^{-29}$ J·m. As shown in Fig. 2(a), the background decreases monotonically with the twist angle, which is in agreement with experiments and our previous work.[21] However, compared to our previous work, μ is larger at present. Accordingly, the peak corresponding to the divergence of A_3 shifts to $\sim 1.3^\circ$ and the intensity is considerably strong. It can be explained as follows: According to Eqs. (3) and (5), the twist angle α corresponding to the resonance condition $(1 + {\rm i}m\gamma(\alpha)/(\hbar^2 k_{0z}^-) \to 0)$ decreases with chemical potential μ. Since the chemical potential μ at present is larger than that of our previous work,[21] the position of the peak will shift towards to smaller twist angle. On the other hand, according to Eqs. (3) and (5), the minimum of $|k_{0z}^-|$ will decrease with μ. Furthermore, the numerator $\exp({\rm i}k_{0z}^- \cdot d_1)$ of the amplitude A_3 will increase with μ, and thus strengthen the peak intensity. Therefore, the peak corresponding to the divergence of A_3 is much stronger than that in our previous work.[21] In addition, compared to our previous work, the peak corresponding to the divergence of A_3 becomes smoother and the peak width becomes larger. This is because the amplitude A_3 at present cannot be divergent for the small-angle incident electrons due to larger chemical potential, which can be easily known from Eqs. (2), (3) and (5). That is to say, these tunneling electrons cannot resonate with the interface potential. Accordingly, the resonance of the scattering is inhibited. Interestingly, when μ increases from 8.0 eV to 8.1 eV, there appears another peak at $\sim 2.5^\circ$ besides the peak corresponding to the divergence of A_3, which can be clearly seen in the inset of Fig. 2(a). That is to say, the peak structure transforms from a single peak to double peaks with the variation of μ. Through numerical analysis, the appearance of the second peak is attributed to the divergence of A_2 (i.e., the resonance caused by the partial wave of $\boldsymbol{k}_{\rm h}^+$). So far, the multiple-peak structure mentioned above can be realized for the present parameter. When μ further increases to 8.2 eV, the peak structure returns to single peak. In order to explain this phenomenon, we have performed the numerical analysis for the interlayer conductance at $\mu = 8.2$ eV, which is shown in Fig. 2(b). From Fig. 2(b), it can be concluded that, for the case of $\mu = 8.2$ eV, the single peak is the superposition of the A_2 peak and the A_3 peak. That is to say, the two peaks overlap with each other, and cannot be distinguished.

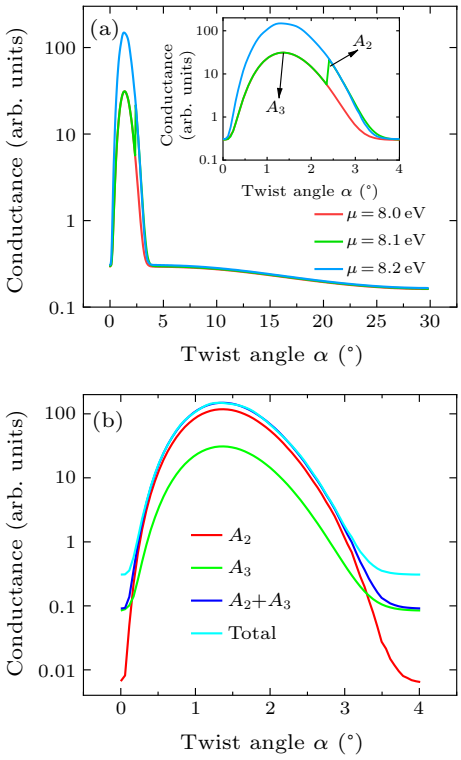


Fig. 2. (a) Interlayer conductances as functions of the twist angle α under different chemical potentials μ. (b) Contributions of the A_2 peak and A_3 peak to the interlayer conductance at $\mu = 8.2$ eV.

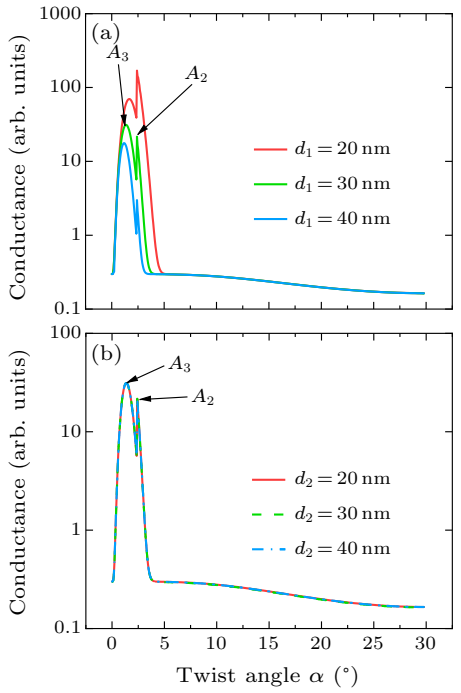


Fig. 3. Interlayer conductances as functions of the twist angle α under different (a) d_1 and (b) d_2.

Secondly, we investigate the influences of the thickness of the Moiré superlattice on the interlayer conductance. Figures 3(a) and 3(b) are the curves of the interlayer conductance versus twist angle under different thicknesses of the upper layer (d_1) and the lower layer (d_2), respectively, where $\mu = 8.1$ eV, $v(\boldsymbol{K}_\mathrm{h}) = 3.5$ eV, $v(0) = 3.12$ eV, and $\gamma_0 = 4 \times 10^{-29}$ J·m. In Fig. 3(a), d_2 is fixed at 30 nm, and in Fig. 3(b), d_1 is fixed at 30 nm. It can be seen from Fig. 3(a) that both the intensities of the two peaks decrease with d_1. According to Eqs. (1) and (2), the attenuation of the intensities originates from the decay factors $\exp(\mathrm{i}k_{0z}^{-} \cdot d_1)$ and $\exp(\mathrm{i}k_{hz}^{+} \cdot d_1)$ in the amplitudes. Furthermore, it can be found that the attenuation of the intensity of the second peak (corresponding to the divergence of A_2) is stronger than the first peak (corresponding to the divergence of A_3). This can be explained as follows: since $\gamma(\alpha) = \gamma_0[1 - \cos(6\alpha)]$, the greater the α, the larger the $\gamma(\alpha)$. As shown in Figs. 2(a) and 3, the resonance angle of the second peak α_2 is greater than that of the first peak α_1, and therefore, $\gamma(\alpha_2) > \gamma(\alpha_1)$. According to the resonance condition $1 + \mathrm{i}m\gamma(\alpha_1)/(\hbar^2 k_{0z}^{-}) \to 0$ and $1 + \mathrm{i}m\gamma(\alpha_2)/(\hbar^2 k_{hz}^{+}) \to 0$, the $|k_{hz}^{+}|$ at the resonance point is larger than $|k_{0z}^{-}|$. Due to the decay factors $\exp(\mathrm{i}k_{hz}^{+} \cdot d_1)$ and $\exp(\mathrm{i}k_{0z}^{-} \cdot d_1)$, the second peak decays more rapidly than the first peak with the increase of d_1. Figure 3(b) indicates that d_2 has little effect on both the peaks. As has been pointed out in Ref. [21], this is due to the fact that the amplitudes of transmitted wave function of the tunneling electron are independent of d_2, which can be known from Eqs. (1) and (2).

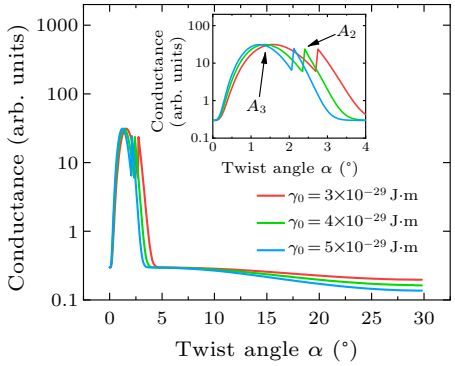


Fig. 4. Interlayer conductances as functions of the twist angle α under different γ_0.

For practical devices, the strength of the interface potential of the Moiré superlattices can be regulated through physical conditions such as applied stress. Thus, it is necessary to discuss the influences of the strength of the interface potential on the interlayer conductance. Figure 4 displays the curves of the interlayer conductance versus twist angle under different γ_0, where $\mu = 8.1$ eV, $v(\boldsymbol{K}_\mathrm{h}) = 3.5$ eV, $v(0) = 3.12$ eV, and $d_1 = d_2 = 30$ nm. As shown in Fig. 4, both the peaks shift towards to the smaller twist angle as γ_0 increases. This can be interpreted as follows: the $\gamma(\alpha)$ corresponding to the resonance is invariant under different γ_0. Since $\gamma(\alpha) = \gamma_0[1 - \cos(6\alpha)]$, the larger the γ_0, the smaller the resonance angle. The above mathematical interpretation corresponds to the following physics: when γ_0 increases, the strength of the interface potential will become stronger at the same twist angle. Physically, it will need smaller twist angle to achieve the resonance of scattering of the tunneling electrons with interface potential. In addition, it can be found that

the background decreases with the increase of γ_0. This can be easily understood such that the stronger interface potential will decrease the amplitudes of transmitted waves, and further decrease the transmission coefficient.

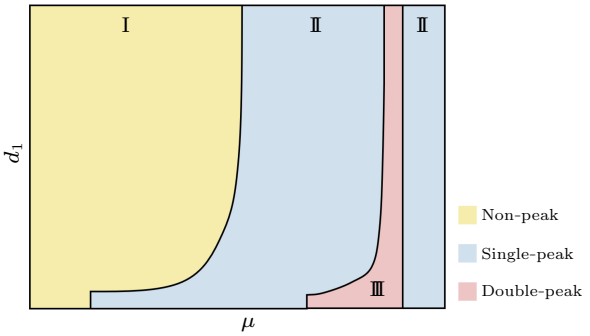


Fig. 5. Phase diagram of the parameter dependence of the peak structure.

Finally, we would like to conclude the parameter dependence of the peak structure, as shown in Fig. 5. It not only includes the present results but also the previous one.[21] In Fig. 5, there are three types of regions: (1) For yellow region I, there is no peak in the curve of interlayer conductance. (2) For blue region II, there is only one peak in the curve of interlayer conductance. (3) For pink region III, there will be double peaks in the curve of interlayer conductance. On the whole, chemical potential μ is the key parameter for the peak structure of the interlayer conductance. We can determine how many partial waves at the interface will resonate with the interface potential, and further determine how many peaks appear in the curve of interlayer conductance. On the other hand, due to the decay factors $\exp(\mathrm{i}k_{0z}^{-}\cdot d_1)$ and $\exp(\mathrm{i}k_{hz}^{+}\cdot d_1)$, the thickness of the upper layer d_1 will also have effect on the peak structure. For a fixed μ, the double-peak (single-peak) structure can transform into single-peak (non-peak) structure with increasing d_1, as can be seen in Fig. 5. In addition, when the two peaks overlap with each other and cannot be distinguished, the double-peak structure will return to single-peak structure, which corresponds to the region II on the right of region III. It should be pointed out that there may, in principle, exist peak structure of more than two peaks. However, the case then will become much more complicated, which may be considered in the future.

For the tunnel junctions with Moiré superlattices, the peak structure plays a key role in applications. As mentioned in our previous work,[21] the high-conductance state and low-conductance state can be considered as "open" state and "close" state, respectively. In applications, the transformation between open and close can be realized by varying the twist angle between the peak and its vicinity. For the case of double-peak structure, there will exist three states: high-conductance state corresponding to the higher peak, intermediate-conductance state corresponding to the lower peak, and low-conductance state corresponding to the region between the two peaks. In particular, the two peaks are quite close in our theoretical results, which is favorable to the implementation of the transformation. This indicates that the tunnel junctions with Moiré superlattices have potential applications in the field of three-state memories.[23]

4. Conclusions

In summary, we have investigated the peak structure in the interlayer conductance of Moiré superlattices using a tunneling theory developed previously by us. The theory is based on the diffraction physics method, which is distinct from the conventional theories. Thus, we can well take into account the coherence caused by the Moiré superlattices. It is found that there may appear double-peak structure in the curve of the interlayer conductance versus twist angle due to the resonance between the tunneling electrons and the interface potential. Furthermore, the influences of the model parameters on the peak structure are studied. In particular, the parameter dependence of the peak structure is concluded via a phase diagram, and the physical meanings of the phase diagram is formulized. In addition, the potential applications of the double-peak structure is discussed. The present work can outline a complete physical picture and provide a deeper understanding for the interlayer conductance of Moiré superlattices.

Acknowledgments

Project supported by the National Natural Science Foundation of China (Grant No. 11704197) and the Natural Science Foundation of Nanjing University of Posts and Telecommunications (Grant Nos. NY221066 and NY223074).

References

[1] Geim A K and Novoselov K S 2007 *Nat. Mater.* **6** 183
[2] Balandin A A 2011 *Nat. Mater.* **10** 569
[3] Xu M, Liang T, Shi M and Chen H 2013 *Chem. Rev.* **113** 3766
[4] Xia F, Wang H, Xiao D, Dubey M and Ramasubramaniam A 2014 *Nat. Photon.* **8** 899
[5] Chu Y, Liu L, Yuan Y, Shen C, Yang R, Shi D, Yang W and Zhang G 2020 *Chin. Phys. B* **29** 128104
[6] McGilly L J, Kerelsky A, Finney N R, Shapovalov K, Shih E M, Ghiotto A, Zeng Y, Moore S L, Wu W, Bai Y, Watanabe K J, Taniguchi T, Stengel M, Zhou L, Hone J, Zhu X, Basov D N, Dean C, Dreyer C E and Pasupathy A N 2020 *Nat. Nanotechnol.* **15** 580
[7] Li T, Jiang S, Li L, Zhang Y, Kang K, Zhu J, Watanabe K, Taniguchi T, Chowdhury D, Fu L, Shan J and Mak K F 2021 *Nature* **597** 350
[8] Tang K and Qi W 2020 *Adv. Funct. Mater.* **30** 2002672
[9] Wang S, Song J, Sun M and Cao S 2023 *Nanomaterials* **13** 2881
[10] Cao Y, Fatemi V, Demir A, Fang S, Tomarken S L, Luo J Y, Sanchez-Yamagishi J D, Watanabe K, Taniguchi T, Kaxiras E, Ashoori R C and Jarillo-Herrero P 2018 *Nature* **556** 80
[11] Cao Y, Fatemi V, Fang S, Watanabe K, Taniguchi T, Kaxiras E and Jarillo-Herrero P 2018 *Nature* **556** 43
[12] Yoo H, Engelke R, Carr S, Fang S, Zhang K, Cazeaux P, Sung S H, Hovden R, Tsen A W, Taniguchi T, Watanabe K, Yi G C, Kim M, Luskin M, Tadmor E B, Kaxiras E and Kim P 2019 *Nat. Mater.* **18** 448

[13] Chung T F, Xu Y and Chen Y P 2018 *Phys. Rev. B* **98** 035425
[14] Liao M, Wu Z W, Du L, Zhang T, Wei Z, Zhu J, Yu H, Tang J, Gu L, Xing Y, Yang R, Shi D, Yao Y and Zhang G 2018 *Nat. Commun.* **9** 4068
[15] Yu Z, Song A, Sun L, Li Y, Gao L, Peng H, Ma T, Liu Z and Luo J 2020 *Small* **16** 1902844
[16] Koren E, Leven I, Lörtscher E, Knoll A, Hod O and Duerig U 2016 *Nat. Nanotechnol.* **11** 752
[17] Chari T, Ribeiro-Palau R, Dean C R and Shepard K L 2016 *Nano Lett.* **16** 4477
[18] Inbar A, Birkbeck J, Xiao J, Taniguchi T, Watanabe K, Yan B, Oreg Y, Stern A, Berg E and Ilani S 2023 *Nature* **614** 682
[19] Kim Y, Yun H, Nam S G, Son M, Lee D S, Kim D C, Seo S, Choi H C, Lee H J, Lee S W and Kim J S 2013 *Phys. Rev. Lett.* **110** 096602
[20] Li H, Wei X, Wu G, Gao S, Chen Q and Peng L M 2018 *Ultramicroscopy* **193** 90
[21] Fang H and Xiao M 2021 *ACS Appl. Electron. Mater.* **3** 2543
[22] Chung D D L 2002 *J. Mater. Sci.* **37** 1475
[23] Capasso F, Sen S, Cho A Y and Sivco D 1987 *IEEE Electron Device Lett.* **8** 297